

Structural colour using organized microfibrillation in glassy polymer films

Masateru M. Ito^{1,2,4*}, Andrew H. Gibbons^{1,3,4}, Detao Qin^{1,2}, Daisuke Yamamoto¹, Handong Jiang^{1,2}, Daisuke Yamaguchi^{1,2}, Koichiro Tanaka^{1,3} & Easan Sivaniah^{1,2*}

The formation of microscopic cavities and microfibrils at stress hotspots in polymers is typically undesirable and is a contributor to material failure. This type of stress crazing is accelerated by solvents that are typically weak enough not to dissolve the polymer substantially, but which permeate and plasticize the polymer to facilitate the cavity and microfibril formation process^{1–3}. Here we show that microfibril and cavity formation in polymer films can be controlled and harnessed using standing-wave optics to design a periodic stress field within the film⁴. We can then develop the periodic stress field with a weak solvent to create alternating layers of cavity and microfibril-filled polymers, in a process that we call organized stress microfibrillation. These multi-layered porous structures show structural colour across the full visible spectrum, and the colour can be tuned by varying the temperature and solvent conditions under which the films are developed. By further use of standard lithographic and masking tools, the organized stress microfibrillation process becomes an inkless, large-scale colour printing process generating images at resolutions of up to 14,000 dots per inch on a number of flexible and transparent formats^{5,6}.

If a standing-wave light pattern is formed in a photosensitive polymer film, then the polymer will be selectively crosslinked in alternating layers in the film (Extended Data Fig. 1). Crosslinking of these layers leads to residual stresses that build across the non-crosslinked layers of the polymer. From our observations, we deduce that when such a film is exposed to a weak solvent, the stresses acting on the non-crosslinked layers will trigger microfibril formation to generate porous layers in the non-crosslinked regions (Fig. 1a), and an overall alternation of these microfibril layers with compact polymer layers.

This structure can be obtained in polystyrene thin films spincoated on silicon wafers that have been crosslinked under high-energy ultraviolet light. Spin-casting is known to leave residual stress in the thin films; these polystyrene films are de-stressed by annealing at high temperature (190 °C) before any ultraviolet exposure. When the exposed film is submerged in acetic acid, which acts as a weak solvent for polystyrene, stepwise changes in film colour are observed as the layers of microfibrils form (Extended Data Fig. 2).

Understanding this structure formation process during immersion in acetic acid is key to using it in future applications. Through scanning electron microscope (SEM) snapshots of the structure, the upper parts of the film are first seen to expand, until a fully open multilayer structure is produced. However, with further exposure to solvent, the upper layers begin to collapse until the entire film is fully closed again (Fig. 1b–e).

The most open form of the structure is highly periodic and composed of alternating dense and porous layers (Fig. 1c). The multi-layered microfibrils provide the useful property of structural colour, as observed by a Bragg peak in the film spectrum (Extended Data Fig. 3a)⁷. Optical transfer matrix analysis verifies the thicknesses of the photonic multilayer structure, 52 nm and 55 nm for the solid and microfibril layers respectively, and estimates a microfibril layer porosity

of 55% (ref. ⁸). Given that the standing-wave periodicity within the original film, 72 nm, is less than the final structure periodicity, this shows that expansion of the film has occurred during the acetic acid treatment.

This process can be followed by real-time spectroscopy measurements, indicating a characteristic structure formation behaviour during immersion in acetic acid (see Extended Data Fig. 3b–e). The real-time spectra can be analysed to determine the expansion of film thickness under three characteristic conditions (Fig. 1f, Extended Data Fig. 3b–d). During exposure to acetic acid at low temperatures (20 °C), the solvent permeates through each stressed but un-crosslinked layer, plasticizing it, and triggering abrupt microfibrillation of the layer; resulting in sudden increases in the overall film thickness. A staircase shape is observed in the expansion ratio with a step for each layer formed as the acetic acid diffuses from the top of the film to the bottom. If the film is developed at a higher temperature (30 °C), there is an additional relaxation of the plasticized microfibril structures. This leads to the subsequent collapse of the microfibril layers and a decrease in the film thickness. On the other hand, if the crosslinked polymer film is then thermally de-stressed by annealing at 160 °C (well above the glass transition temperature of polystyrene), there is no characteristic stepwise expansion in the film, and it is seen to slowly swell to levels seen in thin films with collapsed microfibrils⁹.

This last observation allows us to identify whether the organized stress microfibrillation process arises from differential stress or from differential swelling caused by the absorption differences between the crosslinked and less-crosslinked layers¹⁰. There is a large difference in the maximum expansion and the expansion rate of the film, depending on whether the thermal de-stressing is carried out below or above the glass transition, indicating that the crosslinking stress has been removed (Fig. 1g, h, Extended Data Fig. 3e, f). Moreover, the characteristic stepwise changes in film expansion disappear upon thermal removal of the film stress. The role of differential swelling cannot be completely discounted, because the acetic acid encounters differently crosslinked layers of polystyrene. However, if we were to assume that the microfibril structures were predominantly caused by differential swelling, it is difficult to explain the observations. In its broadest terms, the fundamental process behind organized stress microfibrillation is the stepwise, solvent-mediated expansion of a sequence of pre-stressed glassy polymer layers. By adjustment of the solvent conditions or the development time, it is possible to prevent subsequent collapse of the layers.

The layer periodicity is a standing-wave phenomenon, so we can alter it by crosslinking with different wavelengths of light. However, polystyrene is photosensitive only below 280 nm (ref. ¹¹). To expand polystyrene's photocrosslinking range, photoinitiators such as phenanthrenequinone (PQ) or 4,4'-bis(diethylamino) benzophenone (BDABP) were mixed into the polymer solution before thin film casting. These modified films were then crosslinked under longer-wavelength light-emitting diode (LED) light, up to 405 nm. We verified the role

¹Institute for Integrated Cell-Material Sciences (iCeMS), Kyoto University, Kyoto, Japan. ²Department of Molecular Engineering, Kyoto University, Kyoto, Japan. ³Department of Physics, Kyoto University, Kyoto, Japan. ⁴These authors contributed equally: Masateru M. Ito, Andrew H. Gibbons. *e-mail: mito@icems.kyoto-u.ac.jp; esivaniah@icems.kyoto-u.ac.jp

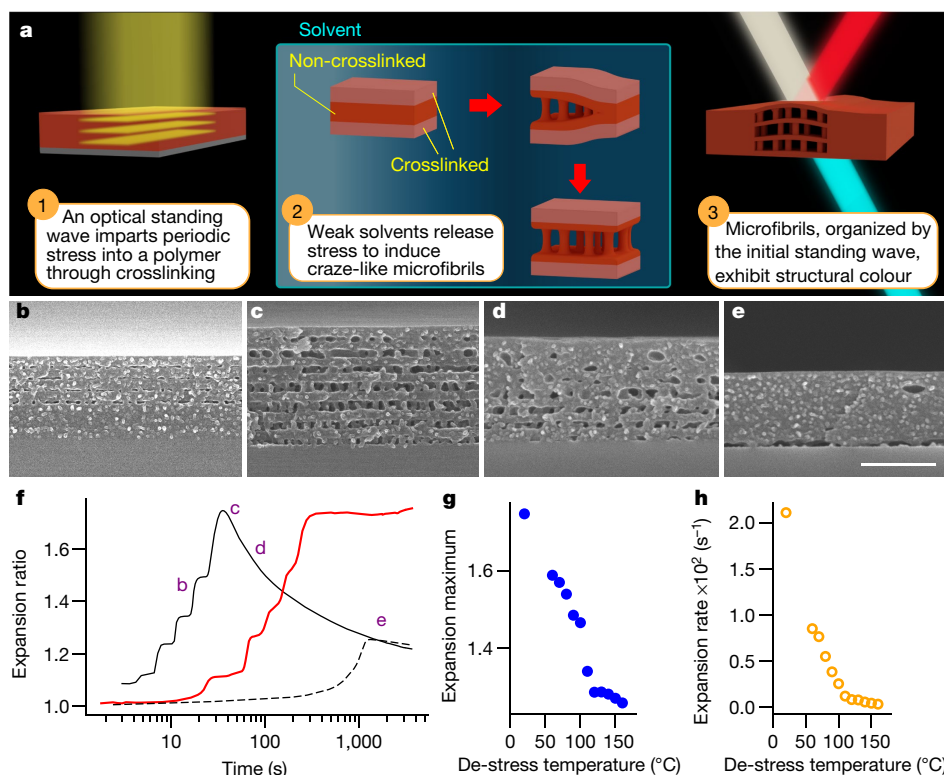


Fig. 1 | Organized stress microfibrillation phenomenon. **a**, Polymer films are crosslinked within a standing-wave pattern to impart internal stress fields. In a weak solvent the stress is released through the formation of microfibrils. The organization of microfibrils generate structural colour properties. **b–e**, Cross-sectional SEM images of 28-kDa polystyrene films crosslinked with wavelengths of 254 nm show the microfibril multilayer structure after different development times in acetic acid at 30 °C. **f**, The ratio between the expanded film thickness and the initial film thickness (the expansion ratio) of films during immersion in acetic acid. Solid black

and red lines refer to polystyrene films developed at 30 °C and 20 °C, respectively; the dashed line refers to a polystyrene film developed at 30 °C, which had first been de-stressed at 160 °C. Time points marked **b–e** in the plot refer to the SEM images in **b–e**. **g, h**, The peak expansion ratio (the expansion maximum) and the expansion rate (the expansion maximum divided by the time taken to reach the expansion maximum) for polystyrene films developed in 30 °C acetic acid after de-stressing at different temperatures. Scale bar for **b–e**, 500 nm.

of standing waves in forming the periodic layers by using polystyrene (PS)/PQ films of varying thickness crosslinked under light of wavelength 375 nm. Over a large range of film thicknesses, 55–1,050 nm, the number of porous layers increased at a regular interval (Fig. 2a), which matched the standing-wave interval of 375-nm light in polystyrene, 114 nm (Fig. 2b).

A range of LEDs of different wavelengths were used to crosslink the light-sensitive polystyrene films (of weight-averaged molecular weight 16 kDa). After development in acetic acid the resulting films had periodic structures and a Bragg peak whose position increased with increasing wavelength of the illumination light (Fig. 2c). The organized stress microfibrillation process was achieved with wavelengths of 285–405 nm in polystyrene. Changing the molecular weight of the polymer (to 160 kDa) results in a blueshift in the Bragg peak position (Fig. 2d, e). If the microfibrils can be associated with the production of crazing, this trend should be expected given that classic craze morphology forms more easily in lower-molecular-weight polymers^{12,13}.

The combined effect of increased illumination wavelength and the microfibril expansion increases the layer spacing of the periodic structure, pushing the Bragg peak into the visible light spectrum. The result is films with vivid structural colour^{14,15}. Even though the maximum illumination wavelength used was 405 nm, the films achieve colours that span the visible light spectrum, over 700 nm (Fig. 2d).

The organized stress microfibrillation process has been generalized to different molecular weights and illumination wavelengths within polystyrene films developed in acetic acid. To establish that this process can be generalized to other glassy polymers, we investigated a selection of frequently used polymers: bisphenol A polycarbonate, poly(methyl methacrylate) (PMMA), and polysulfone (PSF). Thin films of each

polymer were prepared, with BDABP added as the photoinitiator. Although our studies were initiated with PQ, it was found that BDABP was the more versatile photoinitiator in terms of its miscibility in other polymers, and it also had more efficient absorption at high wavelengths, leading to lower crosslinking times. The films were crosslinked under varying wavelengths of LED light and the porous layers were developed in solvents or solvent mixtures, such as acetic acid for polycarbonate, acetic acid and water for PMMA, and acetone and methanol for PSF. Microfibril multilayers could be formed in each of these polymers under different wavelengths of light (Fig. 3a–d).

Fracture in amorphous un-crosslinked glassy polymers is the result of the formation of crazes, which originate in points at which there is a triaxial stress state. If such stress is present, the crazes then grow and eventually give rise to fracture. In the presence of some substances, the onset of crazing occurs at lower stresses and their growth is faster. This phenomenon is called environmental stress crazing. In Hansen solubility theory, the solubility of a polymer/solvent pair can be characterized by a single value, the relative energy difference, where values of relative energy difference less than unity correspond to solvents that are likely to dissolve the polymer¹⁶. Crazing via environmental stress crazing is thought to occur when the polymer is exposed to solvents within a range of relative energy difference and molar volume values^{2,17}, where such values could be considered to represent the thermodynamic and kinetic conditions necessary for environmental stress crazing. Solvent systems with varying relative energy difference and molar volume were prepared and used to develop different polymer films. For each polymer, suitable solvent mixtures were identified that lie within a small region of the relative energy difference and molar volume parameter space (Extended Data Fig. 4). This similarity of solvent grouping to

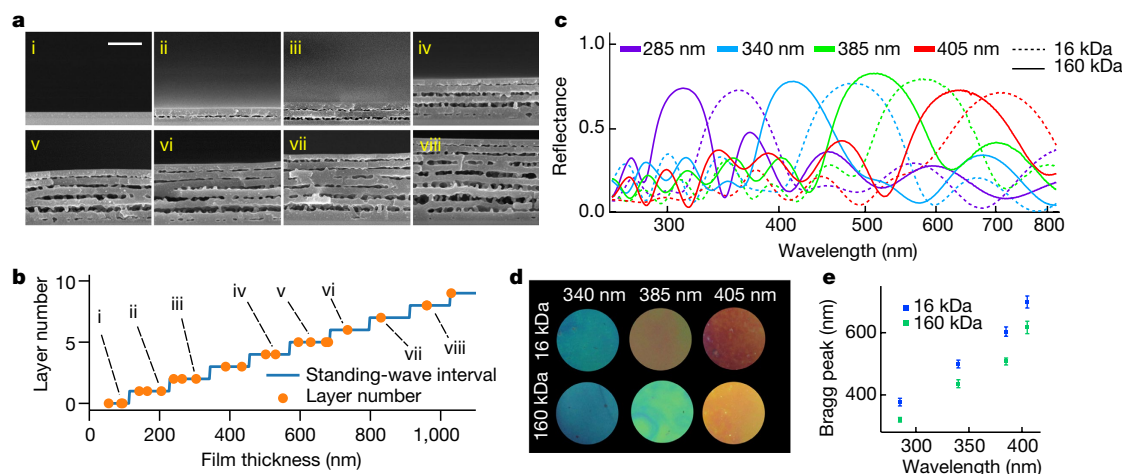


Fig. 2 | Structure from standing-wave interference. **a**, 35-kDa PS/PQ films of varying thickness were used to make organized microfibrillation structures. **b**, The number of porous layers in the films increases at regular intervals as the initial film thickness increases. This interval is equal to that of a standing wave within the as-cast films under 375-nm light, as indicated by the staircase function. **c**, The Bragg peak position of the microfibril structure for 16-kDa PS/PQ and 160-kDa PS/PQ increases

as the illumination wavelength increases. **d**, Films corresponding to the spectra in **c** demonstrate a range of structural colour from blue to red. **e**, Bragg peaks from lower-molecular-weight (16 kDa) polystyrene show that these films have greater expansion than the higher-molecular-weight (160 kDa) films. Error bars show one standard deviation with $n = 5$. Scale bar in **a**, 500 nm.

that observed in environmental stress crazing makes it plausible that the organized stress microfibrillation process shares characteristics with the general phenomenology of fracture in polymers. However, to establish that microfibrils are thus connected to crazing will require further characterization of the stress state in the films.

The organized stress microfibrillation process generates structural colour, and hence could be used to make images in polymer films. Using shadow masks, the illuminated region can be controlled to produce coloured images; by applying a different mask for each wavelength, multiple colour images can be created within the same film (Fig. 4a). For convenience, shadow masks can be generated by simple printing on traditional overhead transparency sheets. The printing process can also be applied to polymer films on transparent substrates (such as glass and polyester film). However, the standing-wave ratio is low for such systems (for example, 1.25 for polystyrene on polyethylene terephthalate (PET) at 375 nm) compared to the standing-wave ratio of polystyrene on Si (3.4 at 375 nm). The overall brightness of the structural colour on transparent substrates can be improved by placing the transparent substrate with the polymer film face down in contact with a silicon wafer so that irradiating light passes through the transparent substrate (Fig. 4b, c). However, uniform contact between the polymer film and silicon is difficult to achieve by this method. A comparison of the transmitted and reflected colour images on the transparent support

confirms that the colour thus generated is the result of bandgap reflections (Extended Data Fig. 5).

Masks made by conventional printing are limited by the resolution of the printer. Micrometre-level printing capability can be achieved using micro-LED illumination, thereby producing high-resolution images (Fig. 4d–l, Extended Data Fig. 6). Films with greater thickness can be used to minimize thin-film colour and to increase the colour contrast in the film (Fig. 4e). Using micro-LED illumination, feature sizes down to 2 μm can be achieved, as demonstrated using the US Airforce Resolution chart (Fig. 4j–l). Prints of periodic lines can achieve feature sizes of 1.8 μm or 14,000 dots per inch (Extended Data Fig. 6e).

Given the key role that thin-film stress plays in this microfibrillation process, it is unsurprising to see the influence of the residual stress from spin casting⁹. Therefore the image of the *Mona Lisa* painting, in which the film was prepared with a casting solvent of chloroform, as opposed to dichloromethane, shows larger variation in the colour (Fig. 4e, f). The colour change is also influenced by the feature size, as can be seen in the resolution chart (Fig. 4j–l). The feature-size colour effect was examined by printing images with pixel sizes of 20 μm and 10 μm . The resulting films have colours that differ according to the pixel size (Fig. 4g–i). Atomic force microscope surface probing shows that this effect is explained by the difference in expansion height between the two films; the 10- μm pixels did not expand as much as the 20- μm pixels,

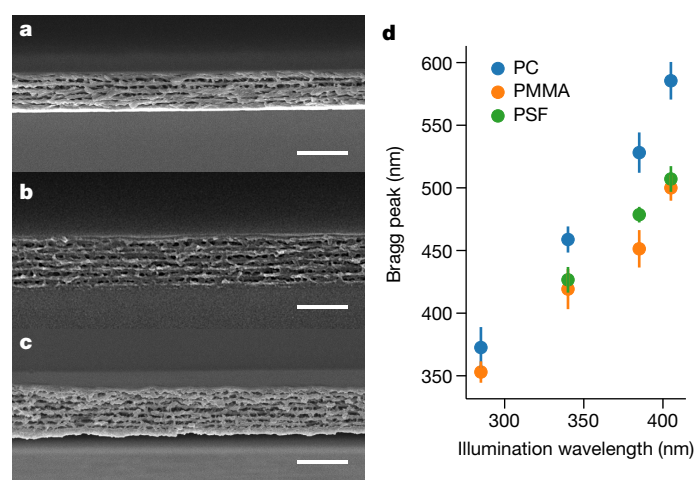


Fig. 3 | Organized stress microfibrillation in other polymers.

The microfibrillation structures can be formed in other polymers such as polycarbonate (in PC/BADBP) (**a**), poly(methyl methacrylate) (in PMMA/BADBP) (**b**), and polysulfone (in PSF/BADBP) (**c**). **d**, Bragg peak position versus illumination wavelength for polycarbonate, PMMA and PSF. Error bars show one standard deviation with $n = 5$. Scale bar for **a–c**, 1 μm .

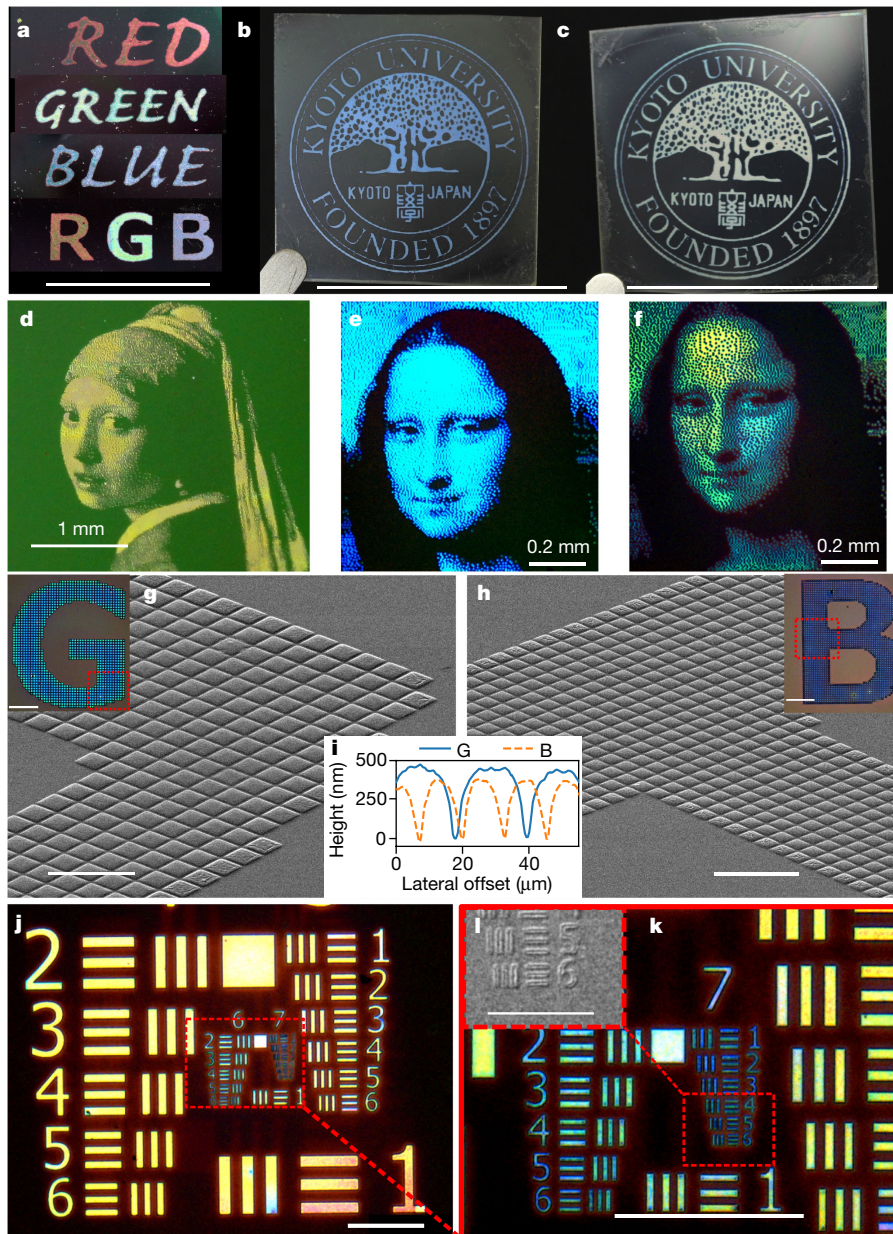


Fig. 4 | Applications of organized stress microfibrillation method.

a, Overhead projector shadow masks were used to generate the red, green and blue text in 35-kDa PS/PQ using 405-nm, 385-nm and 340-nm light, respectively. Thin polydimethyl siloxane (PDMS) sheets were used to isolate structural colour from thin-film interference colour. **b, c**, Structural colour images printed in 192-kDa PS/BDABP on transparent PET substrates with 340-nm light (**b**) and 385-nm light (**c**). **d**, Image of the *Girl with a Pearl Earring* painting created via micro-LED illumination of 35-kDa PS/PQ film. **e, f**, Images of the *Mona Lisa* painting created by micro-LED illumination of 192-kDa PS/BDABP film spin-cast with dichloromethane (**e**) and chloroform (**f**). **g, h**, SEM

images of the letters G and B created with 20- μm and 10- μm micro-LED pixels, respectively, in 192-kDa PS/BDABP. The insets show microscopic images. **i**, Atomic force microscopy indicates that the 20- μm pixels have larger expansion than the 10- μm pixels. **j, k**, Optical microscope images of the US Airforce resolution chart in 192-kDa PS/BDABP demonstrates the resolution range achievable from micro-LED printing of organized microfibrillation structures. The region shown in **k** is indicated by the dotted outline in **j**. Similarly, the inset (**l**) shows an SEM image of the outlined region in **k**. Scale bars: **a**, 1 cm; **b** and **c**, 3 cm; **g** and **h**, 50 μm (inset 200 μm); and **j** and **k**, 200 μm ; **l**, 50 μm .

probably because the expansion is pinned by the edges of the pixel. The colour-feature size dependence provides an additional way to introduce colour into films illuminated with monochromatic light.

Chemical transformation of nanoparticles, micelles and photoresists within optical interference fields is the basis of holography technology, with the aim of developing structural colour and microstructural devices^{4,14,18–24}. There has been a recent shift towards using fracture proactively as a mechanism to create the microstructure for such devices^{25–29}. Our design principle uses optically generated stress fields to develop organized, tunable microstructures within polymers.

Online content

Any Methods, additional references, Nature Research reporting summaries, source data, statements of data availability and associated accession codes are available in the online version of the paper at <https://doi.org/10.1038/s41586-019-1299-8>.

Received: 30 July 2018; Accepted: 30 April 2019;

Published online 19 June 2019.

1. Kambour, R. P. Review of crazing and fracture in thermoplastics. *J. Polym. Sci. D* **7**, 1–154 (1973).
2. Robeson, L. M. Environmental stress cracking: a review. *Polym. Eng. Sci.* **53**, 453–467 (2013).

3. Ward, A. L., Lu, X., Huang, Y. & Brown, N. The mechanism of slow crack growth in polyethylene by an environmental stress cracking agent. *Polymer* **32**, 2172–2178 (1991).
 4. Connes, P. Silver salts and standing waves: the history of interference colour photography. *J. Opt.* **18**, 147–166 (1987).
 5. Kumar, K. et al. Printing colour at the optical diffraction limit. *Nat. Nanotechnol.* **7**, 557–561 (2012).
 6. Carroll, K. M. et al. Fabricating nanoscale chemical gradients with thermochemical nanolithography. *Langmuir* **29**, 8675–8682 (2013).
 7. Sakoda, K. *Optical Properties of Photonic Crystals* Vol. 80 (Springer, 2004).
 8. Born, M. & Wolf, E. *Principles of Optics: Electromagnetic Theory of Propagation, Interference and Diffraction of Light* (Elsevier, 2013).
 9. Chung, J. Y., Chastek, T. Q., Fasolka, M. J., Ro, H. W. & Stafford, C. M. Quantifying residual stress in nanoscale thin polymer films via surface wrinkling. *ACS Nano* **3**, 844–852 (2009).
 10. Kang, C. et al. Full color stop bands in hybrid organic/inorganic block copolymer photonic gels by swelling–freezing. *J. Am. Chem. Soc.* **131**, 7538–7539 (2009).
 11. Li, T., Zhou, C. & Jiang, M. UV absorption spectra of polystyrene. *Polym. Bull.* **25**, 211–216 (1991).
 12. Bray, J. C. & Hopfenberg, H. B. The effect of polymer molecular weight on the solvent crazing of polystyrene. *J. Polym. Sci. B* **7**, 679–684 (1969).
 13. Donald, A. M. & Kramer, E. J. Effect of molecular entanglements on craze microstructure in glassy polymers. *J. Polym. Sci. Polym. Phys. Ed.* **20**, 899–909 (1982).
 14. Kolle, M. et al. Mimicking the colourful wing scale structure of the *Papilio blumei* butterfly. *Nat. Nanotechnol.* **5**, 511–515 (2010).
 15. Chung, W.-J. et al. Biomimetic self-templating supramolecular structures. *Nature* **478**, 364–368 (2011).
 16. Hansen, C. M. 50 years with solubility parameters—past and future. *Prog. Org. Coat.* **51**, 77–84 (2004).
 17. Hansen, C. M. & Just, L. Prediction of environmental stress cracking in plastics with Hansen solubility parameters. *Ind. Eng. Chem. Res.* **40**, 21–25 (2001).
 18. Nadal, E. et al. Plasmon-enhanced diffraction in nanoparticle gratings fabricated by in situ photo-reduction of gold chloride doped polymer thin films by laser interference patterning. *J. Mater. Chem. C* **5**, 3553–3560 (2017).
 19. Matsubayashi, A., Fukunaga, K., Tsuji, T., Ataka, K. & Ohsaki, H. Multilayered ordering of the metal nanoparticles in polymer thin films under photoirradiation. *Langmuir* **27**, 733–740 (2011).
 20. Smirnov, J. R. C. et al. Adaptable ultraviolet reflecting polymeric multilayer coatings of high refractive index contrast. *Adv. Opt. Mater.* **3**, 1633–1639 (2015).
 21. Park, S.-G. & Yang, S.-M. Multicolor patterning using holographic woodpile photonic crystals at visible wavelengths. *Nanoscale* **5**, 4110 (2013).
 22. Yuan, L. & Herman, P. R. Laser scanning holographic lithography for flexible 3D fabrication of multi-scale integrated nano-structures and optical biosensors. *Sci. Rep.* **6**, 22294 (2016).
 23. Suzuki, N., Tomita, Y. & Kojima, T. Holographic recording in TiO₂ nanoparticle-dispersed methacrylate photopolymer films. *Appl. Phys. Lett.* **81**, 4121–4123 (2002).
 24. Campbell, M., Sharp, D. N., Harrison, M. T., Denning, R. G. & Turberfield, A. J. Fabrication of photonic crystals for the visible spectrum by holographic lithography. *Nature* **404**, 53–56 (2000).
 25. Nam, K. H., Park, I. H. & Ko, S. H. Patterning by controlled cracking. *Nature* **485**, 221–224 (2012).
 26. Choi, Y. W. et al. Ultra-sensitive pressure sensor based on guided straight mechanical cracks. *Sci. Rep.* **7**, 40116 (2017).
 27. Dubois, V., Niklaus, F. & Stemme, G. Design and fabrication of crack-junctions. *Microsyst. Nanoeng.* **3**, 17042 (2017).
 28. Yang, C. et al. All-solution-processed, scalable, self-cracking Ag network transparent conductor. *Phys. Status Solidi* **215**, 1700504 (2018).
 29. Kim, M., Ha, D. & Kim, T. Cracking-assisted photolithography for mixed-scale patterning and nanofluidic applications. *Nat. Commun.* **6**, 6247 (2015).
- Acknowledgements** We thank D. Hirayama for assistance with sample preparation and the support of K. Kuroda, head of the JST-Presto Sakigake programme. We thank the Analysis Centre at iCeMS, KUIAS, Kyoto University for access to their SEM and confocal microscope. We thank the Nanohub at Kyoto University for access to their clean room facilities and micro-LED. This work was supported by JST-PRESTO (JPMJPR1417) and the central facilities are supported by the World Premier International Research Initiative (WPI), MEXT, Japan.
- Reviewer information** *Nature* thanks Seung Hwan Ko, Shin-Hyun Kim and Marta Rink for their contribution to the peer review of this work.
- Author contributions** M.M.I. and E.S. initiated, managed and planned the overall project. M.M.I. established the printing protocols. A.H.G. developed the microscopy elements of this work. D.Q., D. Yamamoto, D. Yamaguchi and H.J. all performed the experiments. All authors contributed to data analysis and manuscript refinement and preparation.
- Competing interests** The authors declare no competing interests.
- Additional information**
Extended data is available for this paper at <https://doi.org/10.1038/s41586-019-1299-8>.
Supplementary information is available for this paper at <https://doi.org/10.1038/s41586-019-1299-8>.
Reprints and permissions information is available at <http://www.nature.com/reprints>.
Correspondence and requests for materials should be addressed to M.M.I. or E.S.
Publisher's note: Springer Nature remains neutral with regard to jurisdictional claims in published maps and institutional affiliations.

© The Author(s), under exclusive licence to Springer Nature Limited 2019

METHODS

Polymers. Speciality-grade polystyrenes (with weight-averaged molecular weight, M_w , 16 kDa, 28 kDa and 160 kDa, polydispersity < 1.1 as determined by manufacturer) were obtained from Polymer Source. Commercial-grade polystyrenes (M_w , 35 kDa and 192 kDa, polydispersity > 1.5 as measured using a gel permeation chromatograph (GPC), bisphenol A polycarbonate (M_w , 45 kDa, polydispersity > 1.5 as measured with a GPC), poly(methyl methacrylate) (PMMA, M_w , 120 kDa, polydispersity > 1.5 as measured with a GPC), and polysulfone (PSF, M_w , 35 kDa, polydispersity > 1.5 as measured with a GPC) were obtained from Sigma-Aldrich. A photoinitiator 9,10-phenanthrenequinone (PQ) and 4,4'-bis-(diethylamino)-benzophenone (BDABP) were obtained from Tokyo Chemical Industry and Sigma-Aldrich, respectively. Solvents *n*-hexane, toluene, dichloromethane, chloroform, methanol, ethanol, tetrahydrofuran, acetic acid, ethyl acetate and butyl acetate were obtained from Nacalai Tesque. Solvents 1-propanol, 2-propanol, 1-butanol, 1-chloropentane and acetonitrile, and aluminium oxide powder (Brockmann I) were obtained from Sigma-Aldrich. PDMS was obtained from Dow Corning. Deionized water was produced in the laboratory using a Milli-Q Type 1 Ultrapure Water System (Merck-Millipore).

Purification of polymers. Commercial-grade polystyrene, polycarbonate, PMMA and PSF were purified according to the following protocol: 3 g of polymer was dissolved in 50 ml solvent (toluene for polystyrene, chloroform for polycarbonate, PMMA and PSF) and sonicated for 30 min at 50 °C. The solution was filtered through a 0.2- μ m-pore PTFE membrane syringe filter (md Membrane Technologies) with aluminium oxide powder packed into the syringe. The filtrate was mixed with 200 ml deionized water in a flask and vigorously shaken for 1 min. The mixture was left to separate for 20 min after which the water was drained. The water mixing/draining steps were repeated another four times. 200 ml of methanol was added dropwise to the solution to reprecipitate the polymer. The precipitate was filtered (Whatman filter paper, grade 41) for collection. The purified polymer was dried in a vacuum oven for two days at 50 °C and stored in a desiccator.

Formation of organized microfibrillation structures. Three steps are performed in sequence: spin-casting, crosslinking, and solvent development³⁰.

Spin-casting. The prepared polymer/photoinitiator solutions in either dichloromethane or chloroform were sonicated for 20 min and filtered through a 0.2- μ m-pore PTFE membrane syringe filter. Afterwards, polymer solutions were spun-cast on a clean substrate using a spincoater (MS-A100, Mikasa). Spin casting speeds and concentrations (0.5–5 weight per cent polymer in solvent) were adjusted to obtain desired film thicknesses. Photoinitiator content was 6 and 12 weight per cent in the polymer when BDABP and PQ were used, respectively. Silicon wafer (single side polished), $< 100 >$, N-type (Matsuzaki Seisakusyo, FC-100), cover glass (Muto Pure Chemicals), and PET sheets (Lumirror T60, 250- μ m-thick, Toray Industries) were the three typical substrates employed in this study.

Crosslinking. For large-area crosslinking, the spin-cast polymer films were illuminated in crosslinking ovens. The CX-2000 (UVP) oven was used for 254 nm illumination. Custom ovens were constructed for LED light sources (Thorlabs; wavelengths 300, 340, 375, 385, 395 and 405 nm; see Extended Data Fig. 1). For each wavelength, six LEDs were assembled into an array (2 columns \times 3 rows) and fixed to the ceiling of a custom enclosure (height \times width \times length = 10 cm \times 10 cm \times 18 cm). A USB fan (Evercool, UFAN-12) was operated on top of each box to maintain the custom ovens at room temperature during irradiation.

The placement of polymer films during crosslinking depends on the nature of the substrate. Polymer films on a reflective substrate (for example, silicon wafer) were placed flat, face-up towards the light source, while polymer films on a transparent substrate (for example, cover glass or PET sheet) were placed face-down on a mirrored surface (for example, silicon wafer) with irradiating light passing through the transparent substrate.

To make large-scale images in the films, shadow masks were placed on top of the films during the illumination to crosslink according to the mask pattern. The shadow mask can be custom-designed with graphics software and printed onto transparent overhead projector sheets (Folex FX-471P).

For microscale pattern printing, polymer films were exposed to a micro-LED light source (Maskless Lithography Tool D-light DL-1000GS/KCH, Nano System Solutions). The D-light DL1000 is combined with a digital mirror device (Texas Instruments) for controlling the projection area. The digital mirror device is an electro-mechanical system consisting of 1,024 \times 768 micro-mirrors. The on/off state of each mirror can be controlled individually. The individual mirrors reduce and project light onto 1 μ m \times 1 μ m regions through a lens, which compose to produce an exposure area of 1,024 μ m \times 768 μ m as a single frame. Larger images can be stitched together from multiple frames. An LED with wavelength of 405 nm and intensity of 20 mW cm⁻² was used as the light source of the D-light DL-1000. Typical dose amounts varied from 40–160 J cm⁻² and 500 J cm⁻² for BDABP- and PQ-based thin films respectively. Patterns for micro printing were designed with computer-aided design (CAD)

software (L-Edit) (<https://www.mentor.com/tannereda/l-edit>) and transferred to the micro-LED lithography system as the data input. An outline of the CAD image conversion steps can be found in Extended Data Fig. 6.

Development. The crosslinked polymer films were immersed in a suitable weak solvent. Acetic acid was the typical development solvent. Other solvents and solvent mixtures are shown in Extended Data Fig. 4. Solvent development was performed at room temperature (20 °C) unless otherwise stated. The development process was completed based on the observation of colour changes in the polymer film. Upon completion, developed films were removed and dried using an air blower.

Characterization. An SEM (JEOL JSM-7500F) was used to observe polymer film structures. For cross-sectional observation the samples were fractured while submerged in liquid nitrogen. Each sample was coated with 5 nm of osmium via sputter coating (Filgen Osmium Plasma Coater OPC60A). The topography of polymer films was investigated with an atomic force microscope (NanoWizard III, JPK Instruments) in non-contact mode.

A digital single-lens reflex camera (EOS Kiss X5, Canon) with macro-lens (60-mm EFS, Canon) was employed to take photographs of samples. Before taking photographs the camera was white-balanced using an 18% neutral grey card. When we wanted to eliminate the thin-film interference effect and isolate the structural colour, 2-mm-thick PDMS films were placed on top of the films. PDMS films were prepared with a Sylgard 184 kit by the following steps: (1) the base component was mixed well with the crosslinking agent in a ratio of 10/1 (by weight); (2) the solution was degassed in vacuum; and (3) the solution was poured into a Petri dish and allowed to set overnight at 50 °C into a flexible film.

An upright optical microscope (Axioscope A1 MAT, Carl Zeiss) was used to obtain images of the micro-LED printed polymer films. Samples were illuminated from above with a 100-W halogen bulb light source.

Reflectance spectra were acquired using an ultraviolet–visible spectrometer (MCPD-3700, Otsuka Electronics) with a 210–820-nm light source (MC-2530, Otsuka Electronics). Optical analysis software was used to determine the film thickness using the Cauchy equation model⁸. All reflectance spectra were normalized by the substrate (bare silicon wafer).

A GPC (Shimadzu UFLC system) was used to analyse the molecular weight distribution of the polymers. Analysed polymers were dissolved in tetrahydrofuran to a concentration of 0.2 weight per cent.

In situ spectrum measurement. The effects of stress are of interest in the in situ experiments. To remove pre-existing stress in the films, from spin-cast, polystyrene films (M_w , 28 kDa, Polymer Source) were pre-annealed in a custom vacuum hotplate at 190 °C for 2 h and cooled down to room temperature. After crosslinking under 254-nm light the films were thermally de-stressed by post-annealing in the custom vacuum hotplate under varying temperatures for one hour and allowed to cool down to room temperature. One further sample was annealed for much longer (48 h at 160 °C) so that we could observe the limits of thermally de-stressing. The development solvent, acetic acid, was kept at a stable temperature (30 °C or 20 °C) in a glass dish using a hotplate (AS ONE, CHPS-250DN). The reflectance spectra of the polymer films were measured using an ultraviolet–visible spectrometer (CX-2000, Otsuka) in situ during its immersion in acetic acid under continuous mode. The measurement interval was 0.6 s for the initial 10 min and was switched to a 3-s interval for the remaining time. The change in film thickness during development was calculated through the analysis of the in situ spectrum.

Analysis of in situ spectra. The temporal development of the in situ reflection spectrum was modelled and fitted with a two-layer structure of acetic acid and swelling polystyrene. The model is described as follows⁸:

$$I_{\text{power}} = R_{\text{total}} R_{\text{total}}^* \quad (1)$$

$$R_{\text{total}} = (r_{\text{airAA}} + R_f) / (1 - r_{\text{AAair}} R_f) \quad (2)$$

$$R_f = (r_{\text{AAf}} + r_{\text{ISI}} \exp(-2i\theta)) / (1 - r_{\text{fAA}} r_{\text{ISI}} \exp(-2i\theta)) \quad (3)$$

where an asterisk denotes complex conjugation. I_{power} is the power reflection coefficient, R_{total} is the total reflection coefficient of the structure, R_f is the reflection coefficient from the polystyrene/acetic acid interface and θ is the transmission phase change. r_{12} denotes the reflection coefficient at the interfaces between materials 1 and 2, specifically:

$$r_{\text{fAA}} = (n_f - n_{\text{AA}}) / (n_f + n_{\text{AA}})$$

$$r_{\text{AAf}} = -r_{\text{fAA}}$$

$$r_{\text{AAair}} = (n_{\text{AA}} - 1) / (1 + n_{\text{AA}})$$

$$r_{\text{airAA}} = -r_{\text{AAair}}$$

$$r_{\text{fsi}} = (n_f - n_{\text{Si}} + i\kappa_{\text{Si}}) / (n_f + n_{\text{Si}} - i\kappa_{\text{Si}})$$

where the subscripts refer to the materials (air, film, acetic acid and silicon). The refractive index of the expanded film, n_f , is a combination of the polystyrene refractive index and that of acetic acid. It is calculated by the Lorentz–Lorenz equation with the fraction of acetic acid, φ , as the fitting parameter³¹:

$$\frac{n_f^2 - 1}{n_f^2 + 2} = \frac{n_{\text{AA}}^2 - 1}{n_{\text{AA}}^2 + 2} \varphi + \frac{n_{\text{PS}}^2 - 1}{n_{\text{PS}}^2 + 2} (1 - \varphi)$$

where n_{PS} , the refractive index of the polymer (polystyrene), is calculated via the Sellmeier model³², and the refractive index of acetic acid n_{AA} is obtained from experimental values³³. The refractive index of silicon, n_{Si} , and its extinction coefficient, κ_{Si} , are obtained from experimental values³⁴. The expansion ratio is calculated as $1/(1-\varphi)$.

Standing-wave finite difference time domain simulation. The standing-wave behaviour within the films at varying thickness was simulated using the finite difference time domain method³⁵. The open-source software package MEEP was used to perform the simulations³⁶. A one-dimensional domain was used with an incoming monochromatic plane wave (385 nm). Polystyrene was modelled as a layer with thickness varied over a number of simulations; the refractive index of the layer was derived using the Sellmeier model. The silicon substrate was modelled as a layer containing a perfectly matched layer to absorb incoming waves, allowing the silicon to act as a semi-infinite layer.

Standing-wave ratio. The standing-wave ratio is a measure of the contrast of a standing wave and is defined as the ratio between the anti-node peak amplitude and node peak amplitude. Using the Fresnel equation to determine the reflection coefficient, r , the standing-wave ratio can be calculated as $\frac{1+|r|}{1-|r|}$.

Photonic multilayer films. For dried, acetic-acid-free samples, the transfer matrix method is the most analytical way to fit the measured spectra in a physically meaningful way, because we can assume a multilayer model of alternating high- and low-density layers, where the low-density layer corresponds to the fibrillated structure. It allows a relatively accurate approximation of both porosity and layer sizes. The transfer matrix method is applied in a coarse-grained approach to determine the overall film thickness, and its expansion, during immersion in acetic acid.

The developed film structure was modelled as a one-dimensional photonic multilayer. The transfer matrix method was used to model the structure^{8,37}. We assumed that each of the solid layers had the same thickness and that each of the porous layers had the same thickness. The refractive index of the porous layer, n_p , was approximated as the volume-weighted average of the refractive indices of polystyrene and air⁸:

$$n_p = p n_{\text{air}} + (1-p) n_{\text{PS}}$$

where n_{air} is the refractive index of air, n_{PS} is the refractive index of polystyrene and p is the volume fraction of air (the porosity). Model parameters for layer thickness were obtained from SEM cross-sections and were fitted according to the least-squares method where the spectra were fitted in order to deduce the porosity of the films.

Polymer solubility analysis. According to Hansen solubility parameter theory^{2,38}, the solubility of a polymer depends on: the energy from dispersion forces between molecules (δ_D), the energy from dipolar intermolecular forces between molecules (δ_P), and the energy from hydrogen bonds between molecules (δ_H). These three parameters form the three-dimensional Hansen solubility space. A solvent is represented as a point in Hansen space and a polymer is described by a sphere with radius R_0 . The relative energy difference is defined as R_a/R_0 , where $R_a^2 = 4(\delta_{D1} - \delta_{D2})^2 + (\delta_{P1} - \delta_{P2})^2 + (\delta_{H1} - \delta_{H2})^2$ and subscripts 1 and 2 denote a solvent and a polymer, respectively.

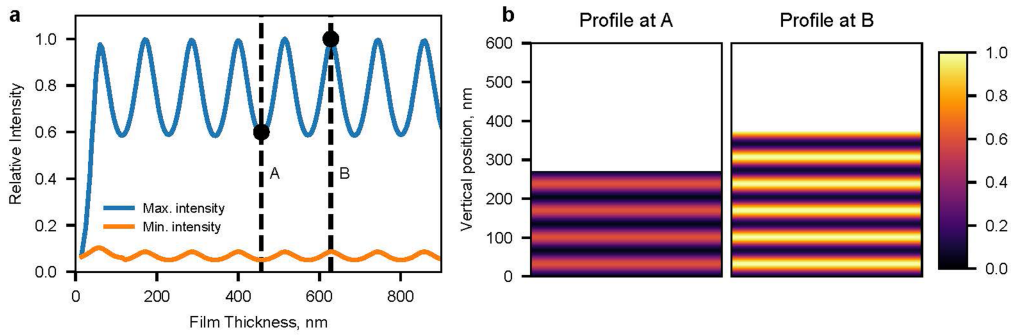
Code availability

The code used for optical analysis in this study is available from the corresponding authors upon reasonable request.

Data availability

The data that supports the findings of this study are available from the corresponding authors upon reasonable request.

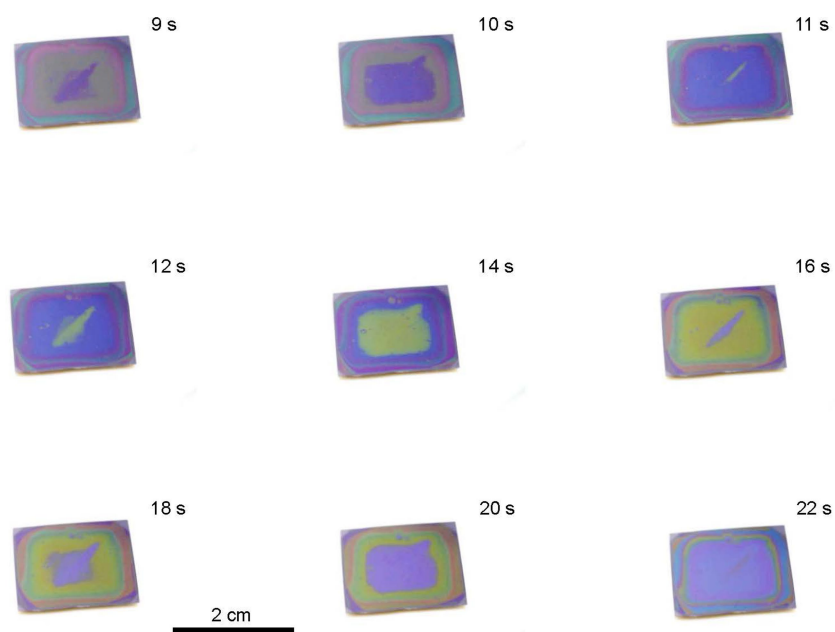
- Thurn-Albrecht, T. et al. Nanoscopic templates from oriented block copolymer films. *Adv. Mater.* **12**, 787–791 (2000).
- Hori, K., Matsuno, H. & Tanaka, K. Sorption kinetics of methanol in thin poly(methyl methacrylate) films studied by optical reflectivity. *Soft Matter* **7**, 10319 (2011).
- Nikolov, I. D. & Ivanov, C. D. Optical plastic refractive measurements in the visible and the near-infrared regions. *Appl. Opt.* **39**, 2067–2070 (2000).
- El-Kashef, H. The necessary requirements imposed on polar dielectric laser dye solvents. *Phys. B* **279**, 295–301 (2000).
- Aspnes, D. E. & Studna, A. A. Dielectric functions and optical parameters of Si, Ge, GaP, GaAs, GaSb, InP, InAs, and InSb from 1.5 to 6.0 eV. *Phys. Rev. B* **27**, 985–1009 (1983).
- Taflove, A. & Hagness, S. C. *Computational Electrodynamics: The Finite-Difference Time-Domain Method* (Artech, 2005).
- Oskooi, A. F. et al. MEEP: A flexible free-software package for electromagnetic simulations by the FDTD method. *Comput. Phys. Commun.* **181**, 687–702 (2010).
- Li, Z.-Y. & Lin, L.-L. Photonic band structures solved by a plane-wave-based transfer-matrix method. *Phys. Rev. E* **67**, 046607 (2003).
- Hansen, C. M. On predicting environmental stress cracking in polymers. *Polym. Degrad. Stab.* **77**, 43–53 (2002).
- Akçay, C., Parrein, P. & Rolland, J. P. Estimation of longitudinal resolution in optical coherence imaging. *Appl. Opt.* **41**, 5256–5262 (2002).
- Wu, D. Y., Meure, S. & Solomon, D. Self-healing polymeric materials: a review of recent developments. *Prog. Polym. Sci.* **33**, 479–522 (2008).



LED central wavelength (nm)	Full width half maximum, $\Delta\lambda$ (nm)	Coherence Length, (μm)
285	13	1.61
300	20	1.17
340	11	2.79
375	9	4.19
385	12	3.33
395	16	2.63
405	12	3.70

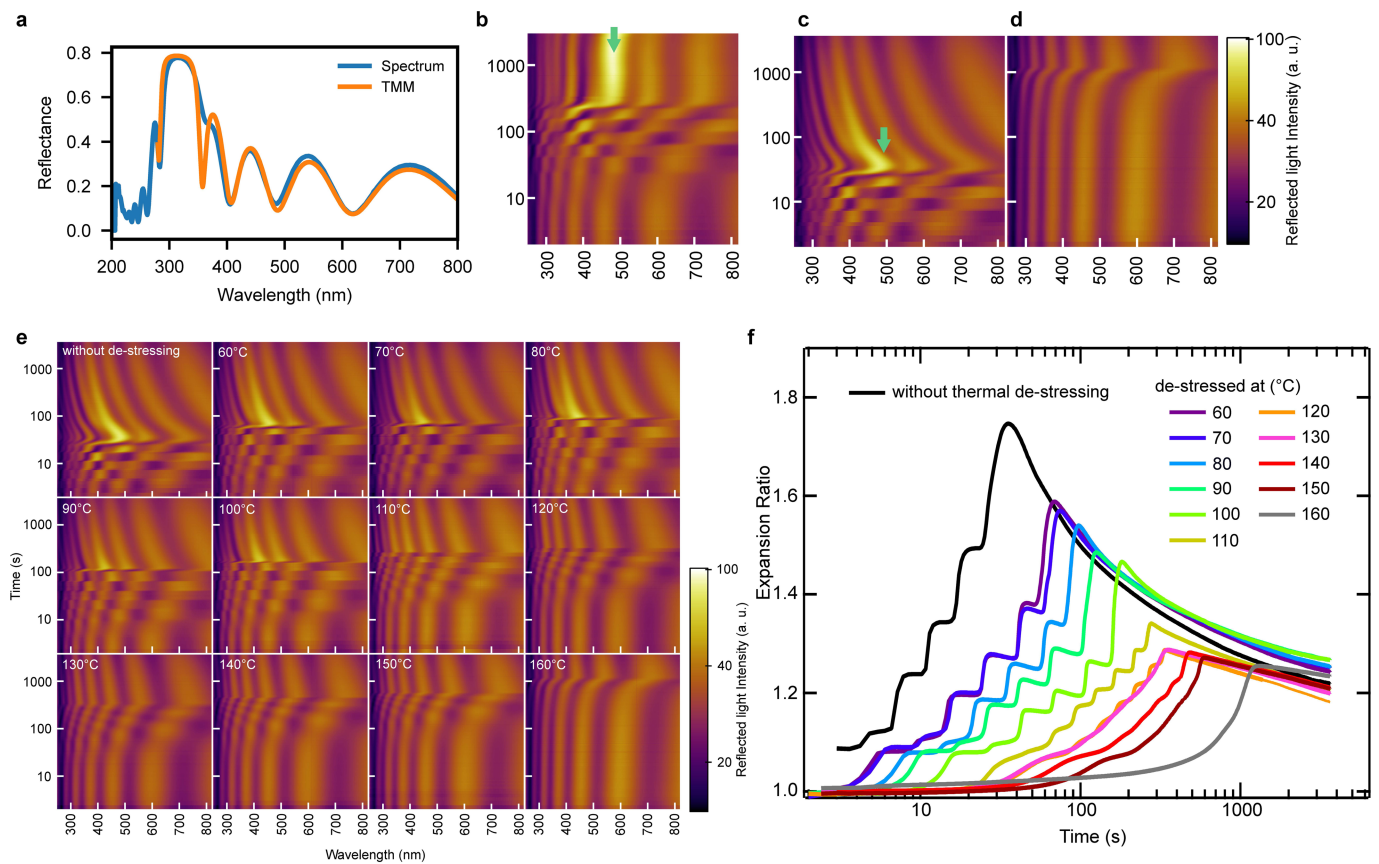
Extended Data Fig. 1 | Standing-wave modelling and light coherence. **a.** Reflecting light within the thin film interferes to form standing waves. As the thickness of the film increases, the minimum intensity remains close to zero while the maximum intensity of the standing wave oscillates within the film, as shown by finite difference time domain simulations of polystyrene on silicon. **b.** Profiles of standing waves in films of different thickness. The colour shows the light intensity relative to the maximum light intensity that can be achieved in this system (the colour scale shows relative light intensity, unitless). At any thickness, for example those indicated by A and B in **a**, standing-wave interference occurs, although the anti-node intensity can vary by a factor of up to 0.6 in this polystyrene

system. Fluctuations in thickness of the thin films therefore do not prevent crosslinking from occurring as long as the applied dose is high enough. The table below outlines the coherence length of the LED light sources used. Approximating Gaussian light sources, the coherence length is $l_c = \sqrt{\frac{2 \ln(2)}{\pi} \frac{\lambda_0^2}{n \Delta \lambda_0}}$ where λ_0 is the free space wavelength of the light source, $\Delta \lambda_0$ is the spectral width (full-width at half-maximum, FWHM), and n is the refractive index of the medium³⁹. The polymer films in this study had thicknesses of less than 1 μm so that coherent interference could be achieved with light sources that have coherence lengths on the micrometre scale.



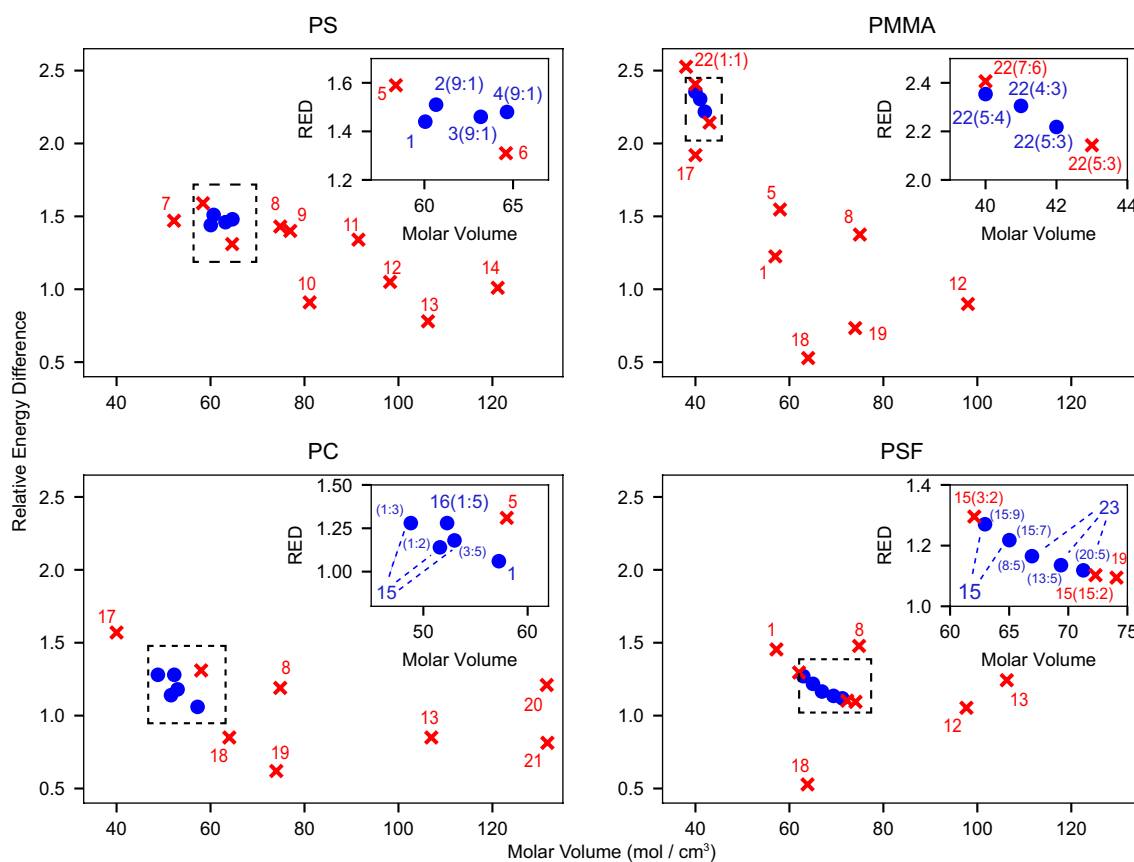
Extended Data Fig. 2 | Colour change during layer formation in acetic acid. Crosslinked polystyrene film (28 kDa) is submerged in acetic acid and porous layers are formed within one minute. Images show snapshots of the stepwise colour change that occurs during the formation of the layers. The time after submersion is indicated in each image. Images were captured using a digital single-lens reflex camera with a macro-lens (EOS

Kiss X5, Canon and 60-mm EFS, Canon); see Supplementary Video 1. We found that the large-scale colour change can begin from any location on the film including the centre (as shown), edges and corners, depending on the local film condition. The final structure and in-plane layer formation dynamics as discussed within this paper are independent of these large-scale colour change effects.



Extended Data Fig. 3 | Spectroscopic analysis of the development of films. **a**, Reflectance spectrum of the developed polystyrene (28 kDa) films and a model photonic multilayer film spectrum produced using the transfer matrix method. **b–d**, Real-time spectroscopy of the immersion process in acetic acid at various conditions. **b**, Polystyrene film crosslinked and developed in an acetic acid bath (20°C). The film initially undergoes a series of sharp changes in spectra, indicating changes in film thickness, and then after formation of a Bragg peak (green arrows), the spectrum persists. **c**, Polystyrene film crosslinked and developed in an acetic acid bath (30°C). Unlike in **b**, the final Bragg peak decays. **d**, Polystyrene film crosslinked, and then annealed at 160°C for 2 days and developed in an acetic acid bath (30°C). The heat map shows a smooth change in spectra, indicating a gradual increase towards a final swollen film without

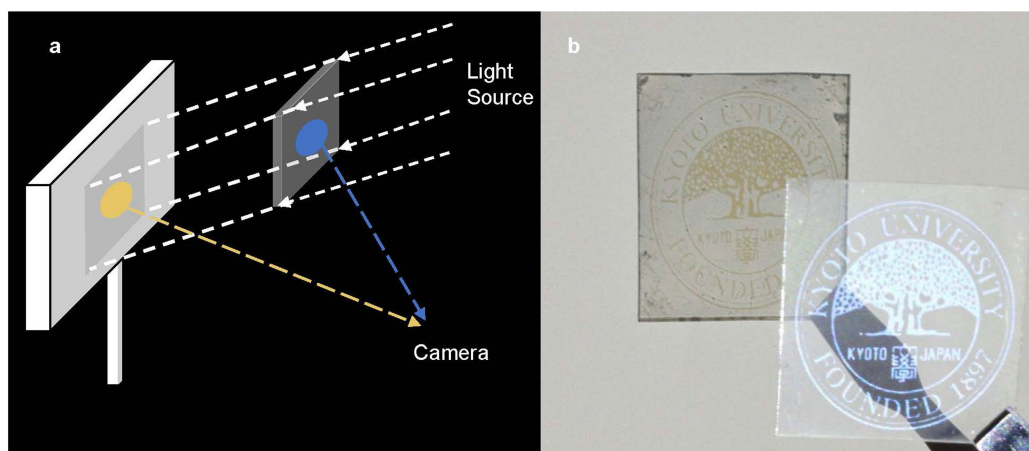
microfibril formation. **e**, After crosslinking, films were post-annealed at a range of temperatures (60–160°C) to remove stresses in the films (thermal de-stressing). Clear stepwise changes in the spectrum are seen in films that were thermally de-stressed below the glass transition temperature (approximately 110°C). After thermal de-stressing at higher temperatures the stepwise expansion effect is reduced and the films simply expand smoothly. **f**, The film thickness expansion over time is derived from real-time spectra where 1.0 corresponds to the initial film thickness. After microstructure expansion finishes the films relax to equilibrium thickness. Without any stress or external force, crazes in glassy polymers undergo collapse under certain conditions⁴⁰, as seen by the decay of the expansion ratio.



No.	Solvent	No.	Solvent
1	Acetic acid	13	Toluene
2	Ethanol / THF	14	1-Chloropentane
3	Ethanol / Toluene	15	Acetone / Methanol
4	Ethanol / 1-Chloropentane	16	Toluene / Methanol
5	Ethanol	17	Methanol
6	Acetonitrile / 1-Propanol	18	Dichloromethane
7	Acetonitrile	19	Acetone
8	1-Propanol	20	Hexane
9	2-Propanol	21	Butyl Acetate
10	THF	22	Acetic Acid / Water
11	Butanol	23	Acetone / Acetic Acid
12	Ethyl Acetate		

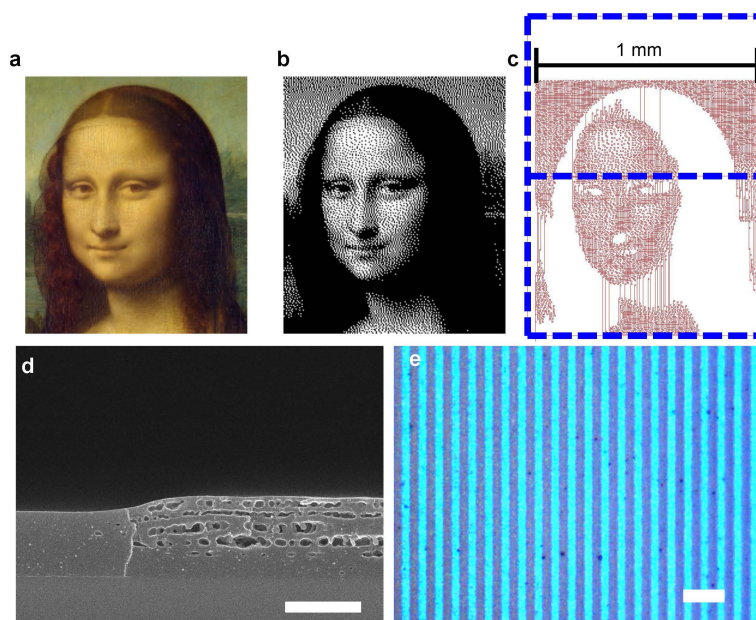
Extended Data Fig. 4 | Hansen parameter plots. Specific solvent conditions associated with Hansen solubility theory were identified for each of the polymers used in this study: polystyrene (PS), PMMA, polycarbonate (PC) and PSF. RED, relative energy difference. The blue dots and red crosses denote successful and unsuccessful application of organized stress microfibrillation respectively. The regions within the

dotted lines are magnified in the insets. The numeric labelling of each solvent is detailed in the corresponding table where the weight ratio of components in a mixture is indicated in parentheses, for example, '16(1:5)' refers to a solution of toluene and methanol with a weight ratio of 1:5. THF, tetrahydrofuran.



Extended Data Fig. 5 | The recording of reflected and transmitted colour. **a**, Illustration for experimental setup to record reflected and transmitted colour of polystyrene film (192 kDa) with BDABP printed on a transparent support. **b**, An example showing reflected and transmitted colour of the Kyoto University logo printed on a PET substrate. A camera

(EOS Kiss X5, Canon) with macro-lens (60-mm EFS, Canon) was used to take the photos. The film reflects blue light and transmits the complementary yellow colour, which can be seen in the shadow of the film. The light source is a 190-W ultrahigh-performance mercury lamp (BenQ, China).



Extended Data Fig. 6 | Micro-LED crosslinking of films. **a, b,** The image to be printed is turned into a two-tone image with Floyd–Steinberg dithering using GIMP software (<https://www.gimp.org/>) (**b**). **c,** The image is then converted to a CAD file using Tanner L-Edit IC Layout software (Mentor Graphics, <https://www.mentor.com/tannereda/l-edit>). The micro-LED system can control the on/off state of an array ($1,024 \times 768$) of $1 \mu\text{m} \times 1 \mu\text{m}$ light sources, which produce a single frame. The dashed grids in **c** indicate how such composite images are divided into individual frames. **d,** An SEM image shows the structure and boundary of a pixel

formed in 35-kDa PS/PQ through micro-LED illumination. Scale bar, $1 \mu\text{m}$. **e,** The image resolution is calculated from the printed stripes (light blue) in 35-kDa PS/PQ, which are $1.8 \mu\text{m}$ wide, corresponding to 14,000 dots per inch. The average linewidths were calculated by first converting the image to a binary image, where the light blue and dark blue were mapped to white and black respectively. The average width of the patterned lines is then calculated as the total area of the white pixels divided by the height of the image and total number of lines. Scale bar, $10 \mu\text{m}$.